

Scalable protocol to mitigate ZZ crosstalk in universal quantum gates

Yan Liang,^{1,2} Ming-Jie Liang,¹ Sai Li,^{1,3} Z. D. Wang,^{4,*} and Zheng-Yuan Xue^{1,3,5,†}

¹Key Laboratory of Atomic and Subatomic Structure and Quantum Control (Ministry of Education), Guangdong Basic Research Center of Excellence for Structure and Fundamental Interactions of Matter, and School of Physics, South China Normal University, Guangzhou 510006, China

²School of Physical Science and Technology, Guangxi Normal University, Guilin 541004, China

³Guangdong Provincial Key Laboratory of Quantum Engineering and Quantum Materials, Guangdong-Hong Kong Joint Laboratory of Quantum Matter, and Frontier Research Institute for Physics, South China Normal University, Guangzhou 510006, China

⁴Guangdong-Hong Kong Joint Laboratory of Quantum Matter, Department of Physics, and HK Institute of Quantum Science & Technology, The University of Hong Kong, Pokfulam Road, Hong Kong, China

⁵Hefei National Laboratory, Hefei 230088, China

(Dated: February 13, 2024)

High-fidelity universal quantum gates are widely acknowledged as essential for scalable quantum computation. However, in solid-state quantum systems, which hold promise as physical implementation platforms for quantum computation, the inevitable ZZ crosstalk resulting from interqubit interactions significantly impairs quantum operation performance. Here we propose a scalable protocol to achieve ZZ -crosstalk mitigation in universal quantum gates. This method converts the noisy Hamiltonian with ZZ crosstalk into a framework that efficiently suppresses all ZZ -crosstalk effects, leading to ideal target quantum operations. Specifically, we first analytically derive the ZZ -crosstalk mitigation conditions and then apply them to enhance the performance of target universal quantum gates. Moreover, numerical simulations validate the effectiveness of ZZ -crosstalk mitigation when multiple qubit gates operate concurrently. As a result, our protocol presents a promising approach for implementing practical parallel quantum gates in large-scale quantum computation scenarios.

I. INTRODUCTION

Quantum computation is an emerging technology that leverages the principles of quantum mechanics to tackle problems that are intractable for classical computation, such as factorization of large integers [1, 2] and database searching [3]. The success of quantum computation relies on the implementation of high-fidelity quantum operations. However, quantum crosstalk in large-scale quantum systems influences parallel quantum operations, leading to error accumulation and propagation [4], which can ultimately cause the quantum computation process to fail. The ZZ crosstalk resulting from interqubit interactions is prevalent in various quantum systems, such as semiconductor and superconducting qubits [5–8], and leads to correlated and nonlocal errors [9, 10], as well as spectator errors [11–13]. Therefore, the development of methods to implement universal quantum gates that can withstand the effects of ZZ crosstalk is crucial, particularly in quantum systems where that effect is significant.

Recently, significant efforts have been devoted to mitigating the ZZ -crosstalk effect in quantum information processing. Firstly, various hardware-based strategies have been proposed, including the integration of tunable couplers or buses [14–21], and the utilization of qubits with opposite anharmonicity [22–24]. However, these strategies heavily rely on the precision of hardware manufacturing, posing substantial challenges. Secondly, quantum control strategies, such as the simultaneous ac Stark effect on coupled qubits [25–29] and dynamical decoupling [30–33], offer alternative approaches

that can alleviate hardware requirements while suppressing ZZ crosstalk. However, due to the lack of freedom of control, the extensibility of the Stark method [25–28] is limited. Besides, the dynamical decoupling method needs to apply the decoupling pulse sequence independently to all spectators to eliminate the ZZ -crosstalk errors [33], resulting in more resource consumption. Recently, an analytical condition for achieving crosstalk-robust control has been proposed [34], which is applicable only to single-qubit cases.

In this paper, we address the above obstacles by presenting a scalable protocol for implementing universal quantum gates with ZZ -crosstalk mitigation (ZZCM) in large-scale quantum systems. The quantum system with a ZZ -crosstalk Hamiltonian is transformed into a framework that suppresses all ZZ -crosstalk effects between qubits, yielding ideal quantum operations. We analytically derive the conditions that the transformed operator must satisfy and apply it to enhance the performance of universal quantum gates. We demonstrate that, for single-qubit gates, the application of a continuous external drive field to the gate qubit can effectively suppress ZZ crosstalk from all nearby qubits, significantly reducing experimental complexity and yielding high-fidelity quantum gates. For parallel quantum gates, the mitigation of ZZ crosstalk between adjacent qubits can be achieved by applying continuous external driving fields only to the next-nearest-neighbor qubits. Furthermore, our scheme does not need additional physical qubits or circuits and is suitable for all quantum processors. Consequently, this approach holds great promise for practical large-scale parallel quantum computation.

* zwang@hku.hk

† zyxue83@163.com

II. QUANTUM GATES WITH ZZCM

In this section, we first present the considered lattice model for universal quantum gates with specification on the explicit form of the ZZ crosstalk. Then, we propose the general scheme for constructing universal quantum gates with ZZCM.

A. ZZ-Crosstalk Model

We consider a general two-dimensional lattice model for scalable quantum computation. Here, scalable quantum computation refers to the ability to efficiently apply our scheme to large-scale quantum systems, requiring only local control, in the presence of residual connections. For demonstration purposes and without loss of generality, we assume the lattice consists of $N \times N$ physical qubits, as depicted in Fig. 1(a). In this lattice, we label the qubit at the i th row and j th column as $Q_{i,j}$. For typical solid-state quantum systems, two nearest-neighbor qubits are coupled through the XY type of interaction [35, 36], and each qubit can be driven independently. The static ZZ coupling is considered as one of the dominant sources of noise [5–8]. The dynamics of the system is governed by the total Hamiltonian $H_t(t) = H_0(t) + H_{zz}$, with $H_0(t) = H_d(t) + H_J(t)$, where $H_d(t)$ represents the Hamiltonian with individual single-qubit drives, $H_J(t)$ describes the interaction between nearest-neighbor qubits of the system, and H_{zz} accounts for the ZZ -crosstalk Hamiltonian. Setting $\hbar = 1$ hereafter, in the interaction picture, the Hamiltonian of a single-qubit under resonant driven is given by

$$H_d(t) = \sum_{i,j} \Omega_{i,j}(t) (\cos \phi_{i,j} \sigma_{i,j}^x + \sin \phi_{i,j} \sigma_{i,j}^y), \quad (1)$$

where $\Omega_{i,j}(t)$ ($\phi_{i,j}$) are the time-dependent driving amplitude (phases) acting on the $Q_{i,j}$ individually, and $\sigma_{i,j} = (\sigma_{i,j}^x, \sigma_{i,j}^y, \sigma_{i,j}^z)$ is Pauli operator. The XY interaction between nearest-neighbor qubits is

$$H_J(t) = \sum_{i,j} \frac{J_{i,j}^x(t)}{2} (\sigma_{i,j}^x \sigma_{i+1,j}^x + \sigma_{i,j}^y \sigma_{i+1,j}^y) + \sum_{i,j} \frac{J_{i,j}^y(t)}{2} (\sigma_{i,j}^x \sigma_{i,j+1}^x + \sigma_{i,j}^y \sigma_{i,j+1}^y), \quad (2)$$

where $\{i, j\} \in \{1, 2, \dots, N\}$ and $J_{i,j}^x(t)$ and $J_{i,j}^y(t)$ being the controllable coupling strength between $Q_{i,j}$ and its nearest-neighbor qubits along the row and column direction, respectively. The adjacent ZZ -crosstalk Hamiltonian is

$$H_{zz} = \sum_{i,j} (\eta_{i,j}^x \sigma_{i,j}^z \sigma_{i+1,j}^z + \eta_{i,j}^y \sigma_{i,j}^z \sigma_{i,j+1}^z), \quad (3)$$

where $\eta_{i,j}^{x,y}$ characterize the coupling strength of ZZ interactions between nearby qubits.

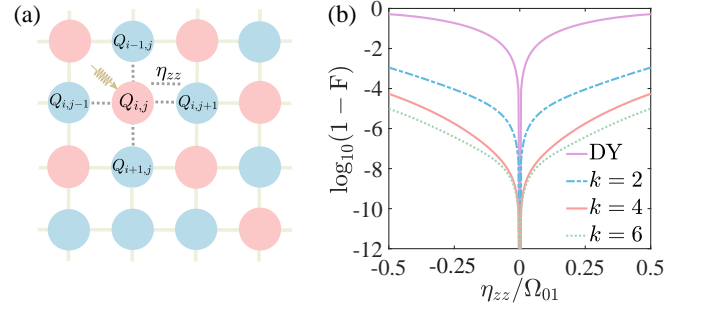


FIG. 1. Construction of single-qubit gate with ZZCM. (a) Schematic illustration on a two-dimensional $N \times N$ physical qubits lattice. (b) Gate infidelity of $\sigma^x/2$ gate on the qubit $Q_{i,j}$ as a function of η_{zz}/Ω_{01} for different values of k . The solid purple line represents the result obtained from the dynamical (DY) scheme.

B. The general scheme

To eliminate the unwanted ZZ crosstalk, we rotate the system to the framework defined by a time-dependent unitary transformation $\mathcal{A}(t)$ as

$$H_{\mathcal{A}}(t) = \mathcal{A}^\dagger(t) H_t(t) \mathcal{A}(t) + i \dot{\mathcal{A}}^\dagger(t) \mathcal{A}(t). \quad (4)$$

Our goal is to devise the form of $\mathcal{A}(t)$ such that the resulting evolution operator of $H_{\mathcal{A}}(t)$ yields an ideal gate operation at the final moment, i.e.,

$$U_{\mathcal{A}}(T, 0) = \mathcal{T} e^{-i \int_0^T H_{\mathcal{A}}(t) dt} = U_0 \quad (5)$$

where \mathcal{T} denotes time ordering, T represents the duration of the gate operation, and U_0 signifies the ideal gate operation free from the influence of ZZ crosstalk. By imposing the boundary condition of $\mathcal{A}(T) = \mathcal{A}(0) = \mathbf{I}$, the evolution operator generated by $H_t(t)$ in the interaction picture can be expressed as

$$U_t(T, 0) = \mathcal{A}(T) U_{\mathcal{A}}(T, 0) = \mathbf{I} \cdot U_0, \quad (6)$$

which implies that we eliminate the adverse effect of ZZ crosstalk and realize the ideal gate operation.

To determine the specific form of $\mathcal{A}(t)$ satisfying Eq. (6), we divide the evolution into k segments (k is a positive integer), that is $T = k\tau$ with k being positive integer, and expand $U_{\mathcal{A}}(T, 0)$ as

$$U_{\mathcal{A}}(T, 0) = \prod_{n=1}^k U_{\mathcal{A}}[n\tau, (n-1)\tau]. \quad (7)$$

For the n th period $U_{\mathcal{A}}[n\tau, (n-1)\tau] = \mathcal{T} \exp \left[-i \int_{(n-1)\tau}^{n\tau} H_{\mathcal{A}}(t) dt \right]$, by using the Magnus expansion [37, 38], the unitary evolution operator $U_{\mathcal{A}}[n\tau, (n-1)\tau]$ corresponding to a time-dependent Hamiltonian is

$$U_{\mathcal{A}}[n\tau, (n-1)\tau] = e^{-i\tau(\bar{H}^{(0)} + \bar{H}^{(1)} + \dots)}, \quad (8)$$

where $\bar{H}^{(j)}$ is characterized by an order of τ^j . Here, we restrict to the first-order term $\bar{H}^{(0)}$, which is known as a lowest-order approximation. It is noteworthy that this approximation becomes exact in the limit of τ is infinitesimal. In practical situations, we impose the condition that τ is significantly smaller than the gate time. In the lowest-order approximation, the evolution operator becomes $U_{\mathcal{A}}[n\tau, (n-1)\tau] = \exp^{-i\tau\bar{H}^{(0)}}$, with

$$\begin{aligned} \bar{H}^{(0)} &= \frac{1}{\tau} \int_{(n-1)\tau}^{n\tau} H_{\mathcal{A}}(t) dt \\ &= \frac{1}{\tau} \left[\int_{(n-1)\tau}^{n\tau} H_{\mathcal{A}0}(t) dt + \int_{(n-1)\tau}^{n\tau} \mathcal{A}^\dagger(t) H_{zz} \mathcal{A}(t) dt \right], \end{aligned} \quad (9)$$

where

$$H_{\mathcal{A}0}(t) = \mathcal{A}^\dagger(t) H_0(t) \mathcal{A}(t) + i\dot{\mathcal{A}}^\dagger(t) \mathcal{A}(t) \quad (10)$$

is the target Hamiltonian without ZZ crosstalk for $H_0(t)$, in the $\mathcal{A}(t)$ framework, which can realize the ideal gate U_0 .

To eliminate the influence of H_{zz} , we impose two conditions to $\mathcal{A}(t)$, i.e.,

$$\mathcal{A}(t) = \mathcal{A}(t + \tau), \quad (11a)$$

$$\int_0^\tau \mathcal{A}^\dagger(t) H_{zz} \mathcal{A}(t) dt = 0, \quad (11b)$$

which indicate that $\mathcal{A}(t)$ is periodic with its period being τ , and the integral of H_{zz} in the framework of $\mathcal{A}(t)$ is zero, within any periods. By these settings, Eq. (7) becomes

$$U_{\mathcal{A}}(T, 0) \approx \prod_{n=1}^k e^{-i \int_{(n-1)\tau}^{n\tau} H_{\mathcal{A}0}(t) dt} \approx U_0, \quad (12)$$

which is the ideal rotation operation. Imposing the boundary condition $\mathcal{A}(T) = \mathcal{A}(0) = \mathbf{I}$, and move back to the interaction picture, we obtain the evolution operator generated by $H_t(t)$ is $U_t(T, 0) = \mathcal{A}(T) U_{\mathcal{A}}(T, 0) = U_0$. Overall, the key to mitigating ZZ crosstalk and realizing ideal quantum gates is to find a transformed operator $\mathcal{A}(t)$ that satisfies the boundary condition $\mathcal{A}(T) = \mathcal{A}(0) = \mathbf{I}$ and Eq. (11).

III. EXAMPLES OF UNIVERSAL QUANTUM GATES

In this section, we exemplify the construction of universal quantum gates with ZZCM in the considered lattice model, which can support scalable universal quantum computation. While our simulations are based on a simplified qubit case, techniques for mitigating gate error induced by low anharmonicity of qubits can also be incorporated in our scheme.

A. Single-qubit gate

As shown in Fig. 1(a), we utilize the construction of a single-qubit $\sigma^x/2$ gate on qubit $Q_{i,j}$ as an example to provide

a detailed explanation of how to eliminate ZZ crosstalk from the surrounding four spectator qubits, i.e., $Q_{i-1,j}$, $Q_{i+1,j}$, $Q_{i,j-1}$, $Q_{i,j+1}$. We start from Eq. (10), where the single-qubit driven Hamiltonian in the framework of $\mathcal{A}_1(t)$ reads

$$H_{\mathcal{A}1}(t) = \Omega_{01}(t) \sigma_{i,j}^x, \quad (13)$$

where $\Omega_{01}(t) = \Omega_{01} \sin^2(\pi t/T_1)$ with Ω_{01} being the pulse amplitude, and T_1 being the gate operation time satisfied $\int_0^{T_1} \Omega_{01}(t) dt = \pi/4$. Note that, our scheme does not impose limitations on the shape of $\Omega_{01}(t)$. Here, we chose $\Omega_{01}(t)$ to be a commonly used time-dependent waveform in experimental settings. This waveform exhibits a continuous transition from zero to zero, minimizing abrupt changes, and has practical advantages in experimental implementation, such as reducing undesirable transients. The nearest ZZ -crosstalk Hamiltonian can be written as

$$H_{zz1} = \eta_{zz} \sigma_{i,j}^z Z_{i,j}, \quad (14)$$

where

$$Z_{i,j} = \sigma_{i-1,j}^z + \sigma_{i+1,j}^z + \sigma_{i,j-1}^z + \sigma_{i,j+1}^z$$

are the summation of the σ^z operators of the four nearest-neighbor qubits for $Q_{i,j}$, and we assume that the ZZ -crosstalk strengths are the same for the sake of simplicity.

For elimination of ZZ crosstalk, we choose the time-dependent transformed operator $\mathcal{A}_1(t)$ to be

$$\mathcal{A}_1(t) = \exp \left[-i \frac{\omega_1 \tau_1}{\pi} \sin^2 \left(\frac{\pi t}{\tau_1} \right) \sigma_{i,j}^x \right], \quad (15)$$

where $\tau_1 = T_1/k$ is the period, and ω_1 being the parameter used to satisfy Eq. (11b). It is obvious that $\mathcal{A}_1(t)$ satisfies the boundary condition $\mathcal{A}_1(0) = \mathcal{A}_1(T_1) = \mathbf{I}$ and Eq. (11a). In addition, the condition in Eq. (11b) can be written as

$$\begin{aligned} & \int_{(n-1)\tau_1}^{n\tau_1} \mathcal{A}_1^\dagger(t) H_{zz1} \mathcal{A}_1(t) dt \\ &= \eta_{zz} \int_{(n-1)\tau_1}^{n\tau_1} (\cos \chi \sigma_{i,j}^z + \sin \chi \sigma_{i,j}^y) Z_{i,j} dt, \end{aligned} \quad (16)$$

where $\chi = 2\omega_1 \tau_1 / \pi \sin^2(\pi t/\tau_1)$. We define the error cumulant during the n th period as

$$\text{EC} = \eta_{zz} \left[\left| \int_{(n-1)\tau_1}^{n\tau_1} \cos \chi dt \right| + \left| \int_{(n-1)\tau_1}^{n\tau_1} \sin \chi dt \right| \right]. \quad (17)$$

Through the numerical simulation, it can be concluded that $\omega_1 = 4.81k\Omega_{01}$ is the optimal choice for making the error cumulant to be zero, see Appendix A for details. Note that, as shown in Eq. (17), η_{zz} appears outside of the integrals. Therefore, as long as the integrals evaluated to be zero over the duration of interest, the error cumulant will be zero, i.e., independent on the value of η_{zz} for different qubits. The assumption of equal η_{zz} for all neighbors is set only for the sake of simplicity and clear representation. Meanwhile, Eq. (17) is applicable for the slowly varying drift case, i.e., $\eta_{zz} \ll 1/\tau_1$, this assumption is held for solid-state quantum systems [29, 39].

Once the form of $\mathcal{A}_1(t)$ is determined, we can obtain the total Hamiltonian $H_1(t)$ in the interaction picture by inverting Eq. (4), i.e.,

$$\begin{aligned} H_1(t) &= \mathcal{A}_1(t)H_{\mathcal{A}_1(t)}\mathcal{A}_1^\dagger(t) + i\frac{d\mathcal{A}_1(t)}{dt}\mathcal{A}_1^\dagger(t) + H_{zz1} \\ &= \Omega_1(t)\sigma_{i,j}^x + H_{zz1}, \end{aligned} \quad (18)$$

with $\Omega_1(t) = \Omega_{01} \sin^2(\pi t/T_1) + \omega_1 \sin(2\pi t/\tau_1)$. Note that, to meet the conditions in Eq. (11) and the boundary condition $\mathcal{A}(T) = \mathcal{A}(0) = \mathbf{I}$, the form of $\mathcal{A}_1(t)$ is not fixed, we choose the sine square form is aimed to set the added waveform, the second term in $\Omega_1(t)$, to be simple sine function. This indicates that we can mitigate the ZZ crosstalk from all spectators only by modulating the shape of the external drive on the gate qubit from $\Omega_{01}(t)$ to $\Omega_1(t)$, and the term $i\dot{\mathcal{A}}_1(t)\mathcal{A}_1^\dagger(t)$ serves as the additional correction Hamiltonian, which consists of only single qubit terms.

It is worth noting that the target ZZCM Hamiltonian in Eq. (10) is consistent with the type of quantum gate under consideration. However, on constructing other types of quantum gates, the target ZZCM Hamiltonian in Eq. (10) will be changed accordingly. In this case, the form of Eq. (15) for $\mathcal{A}_1(t)$ will also be changed in order to suppress ZZ crosstalk. After setting the target ZZCM Hamiltonian and its corresponding $\mathcal{A}_1(t)$, the resulting Hamiltonian in the interaction picture can still be obtained using the formula in the first line of Eq. (18). Generally, the design of $\mathcal{A}(t)$ needs careful consideration to ensure that the Hamiltonian in the interaction picture, namely Eq. (18), possesses concise form and retains practical feasibility.

We numerically quantify the gate robustness by using the gate fidelity of $F(U_0) = |\text{Tr}(U_0^\dagger U_{zz})|/|\text{Tr}(U_0^\dagger U_0)|$ [40], where U_0 and U_{zz} are the ideal and error-affected evolution operators, respectively. Figure 1(b) shows a comparison of the robustness to ZZ crosstalk of ZZCM schemes with different k and the DY scheme, where the DY scheme is implemented by using a pulse of $\Omega_{d1}(t) = \Omega_{01} \sin^2(\pi t/T_{d1})$, with T_{d1} being the gate time, see Appendix B for details. The numerical results reveal a positive correlation between an increase in k and an enhancement of the resilience to ZZ crosstalk. This relationship stems from the fact that, larger k corresponds to smaller $\tau_1 = T_1/k$, which leads to an improved precision of the lowest-order Magnus expansion approximation. This heightened precision in representing the system's dynamics results in a more efficient mitigation of ZZ crosstalk. Additionally, we can observe that the gate infidelity as a function of η_{zz}/Ω_{01} ($\eta_{zz}/\Omega_{01} \in [-0.5, 0.5]$) can be smaller than 10^{-4} throughout the entire range of errors for $k \geq 4$. Notably, compared to the DY scheme, the gate infidelity of the ZZCM schemes reduces by at least 2 orders of magnitude when the error ratio exceeds $|0.02|$.

It is noted that, from a general theoretical perspective, it is true that smaller values of τ_1 (or larger k) lead to a more accurate lowest-order approximation of Magnus expansion, which, in turn, results in a more effective suppression of ZZ crosstalk. However, we can infer from Eq. (18) that the modulated coupling strength $\Omega_1(t)$ increases as k increases, which

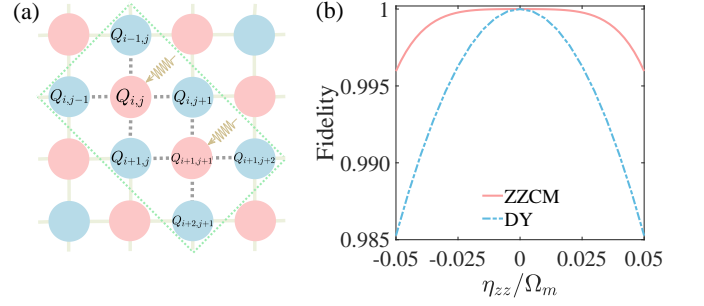


FIG. 2. Construction of parallel single-qubit gate with ZZCM. (a) The lattice structure for constructing single-qubit gates $\sigma_{i,j}^x \otimes \sigma_{i+1,j+1}^y$, i.e., σ^x on qubit $Q_{i,j}$ and σ^y on qubit $Q_{i+1,j+1}$. (b) Gate fidelity of parallel gates as a function of η_{zz}/Ω_m .

is not favorable for implementation in an actual experimental setup. Therefore, when selecting k , one needs to balance the ZZ crosstalk suppression and experimental feasibility for the control pulses. This balance will depend on the specific physical system under investigation. To address this issue, we set the maximum value of $\Omega_1(t)$ as Ω_m , with η_{zz}/Ω_m ranging from -0.05 to 0.05 . Under these conditions, the optimal choice of k is found to be 4, as shown in Appendix C.

B. Parallel single-qubit gates

In the context of scalable quantum computation, parallel quantum gates play a pivotal role. In the absence of ZZ crosstalk, simultaneously constructed single-qubit gates are trivial, which can be induced by independent driving fields. However, in the presence of ZZ crosstalk, parallel single-qubit gates are no longer trivial, as manipulating one of the qubits will also lead to unintended operation on its nearby qubits, leading them to be entangled with gate qubits. Therefore, we now focus on the suppression of interqubit ZZ crosstalk during the construction of parallel single-qubit gates.

Here we take the parallel single-qubit gates σ^x on $Q_{i,j}$ and σ^y on $Q_{i+1,j+1}$ simultaneously as an example, as shown in the dotted box in Fig. 2(a). Note that, parallel single-qubit gates on nearest-neighbor qubits can also be implemented, as detailed in Appendix D. Starting from Eq. (10), the individual single-qubit driven Hamiltonian is

$$H_{A2}(t) = \Omega_{02}(t)(\sigma_{i,j}^x + \sigma_{i+1,j+1}^y) \quad (19)$$

with $\Omega_{02}(t) = \Omega_{02} \sin^2(\pi t/T_2)$, where the gate operation time T_2 satisfies $\int_0^{T_2} \Omega_{02}(t) dt = \pi/2$. In this case, the Hamiltonian of nearest ZZ crosstalk can be written as

$$H_{zz2} = \eta_{zz}(\sigma_{i,j}^z Z_{i,j} + \sigma_{i+1,j+1}^z Z_{i+1,j+1}). \quad (20)$$

When we choose the transformed operator as

$$\mathcal{A}_2(t) = \exp\left[-i\frac{\omega_2 T_2}{\pi} \sin^2\left(\frac{\pi t}{T_2}\right) (\sigma_{i,j}^x + \sigma_{i+1,j+1}^y)\right], \quad (21)$$

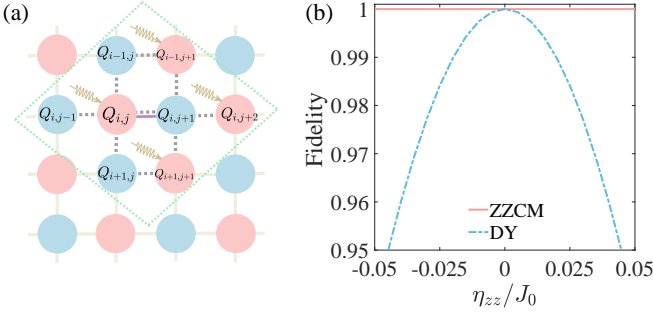


FIG. 3. Simultaneously construction of single- and two-qubit gates with ZZCM. (a) The lattice structure for constructing gates of $U_{(i,j),(i,j+1)}^S \otimes \sigma_{i-1,j+1}^x \otimes \sigma_{i,j+2}^y \otimes I_{i+1,j+1}$, which construct a SWAP gate on qubits $Q_{i,j}$ and $Q_{i,j+1}$, a σ^x gate on qubit $Q_{i-1,j+1}$, a σ^y gate on qubit $Q_{i,j+2}$, and the identity operation on qubit $Q_{i+1,j+1}$, simultaneously. (b) Gate fidelity as a function of η_{zz}/J_0 .

the Hamiltonian in the interaction picture can be obtained by inverting Eq. (4), i.e.,

$$H_2(t) = \Omega_2(t)(\sigma_{i,j}^x + \sigma_{i+1,j+1}^y) + H_{zz2}, \quad (22)$$

where the equivalent coupling strength is $\Omega_2(t) = \Omega_{02} \sin^2(\pi t/T_2) + \omega_2 \sin(2\pi t/\tau_2)$. Here, $\tau_2 = T_2/k$ is the period, and ω_2 is the parameter used to satisfy Eq. (11b). By utilizing numerical simulations, we can determine the optimal value of ω_2 is $2.4k\Omega_{02}$, which ensures the error cumulant to be zero, see Appendix A for details. By setting the maximum value of $\Omega_2(t)$ to Ω_m , and imposing a constraint on η_{zz}/Ω_m in the range of $[-0.05, 0.05]$, we can identify the optimal value of k to be 4. A comparison between the robustness of the ZZCM scheme with $k = 4$ and the DY scheme against ZZ crosstalk is presented in Fig. 2(b), where the DY scheme is implemented by using a pulse of $\Omega_{d2}(t) = \Omega_m \sin^2(\pi t/T_{d2})$, with T_{d2} being the gate time, see Appendix B for details. The results indicate a meaningful increase in robustness for the entire error range when implementing the ZZCM proposal.

C. The two-qubit SWAP gate

Compared to single-qubit gates, two-qubit gates are more susceptible to parasitic ZZ crosstalk, significantly challenging the attainment of high-performance two-qubit gates. Therefore, suppressing ZZ crosstalk is crucial for implementing high-performance two-qubit gates. In this regard, we devise the two-qubit SWAP gate with ZZ -crosstalk mitigation effects. Considering a quantum system consisting of eight physical qubits enclosed in a dotted box in Fig. 3(a), where the SWAP gate $U_{(i,j),(i,j+1)}^S$ are acted on qubits $Q_{i,j}$ and $Q_{i,j+1}$, and the remaining six qubits, $Q_{i-1,j}$, $Q_{i-1,j+1}$, $Q_{i,j-1}$, $Q_{i,j+2}$, $Q_{i+1,j}$, $Q_{i+1,j+1}$, denote the spectators. The interaction between qubits is indicated by the solid and dashed lines, which correspond to the XY and ZZ interactions, respectively.

It is worth noting that, unlike the approach taken for constructing single-qubit gates, when building two-qubit gates,

we follow the general principles outlined in Sec. II, i.e., we start with the Hamiltonian in the interaction picture. When constructing single-qubit quantum gates, we start from the target Hamiltonian in Eq. (13), in the framework of $\mathcal{A}_1(t)$, to obtain the interaction Hamiltonian in Eq. (18) in a reverse way. This reverse approach allows us to establish the relationship between the Hamiltonian in the interaction picture and the rotation operator $\mathcal{A}(t)$. This approach is applicable for single-qubit gate construction, as arbitrary direction of single-qubit control is experimental achievable. However, when constructing two-qubit gates, the form of the two-qubit coupling is in specific forms for different quantum systems. Here, as shown in Fig. 3(a), we consider the conventional XY interactions between nearby qubits, and use only single-qubit operations to suppress ZZ crosstalk. Therefore, we initially set the form of the interaction Hamiltonian, to avoid introducing two-qubit interactions beyond the intended XY coupling. Inspired by Eq. (18), we represent the interaction Hamiltonian as

$$H_3(t) = H_J(t) + H_{zz3} + H_{A3}(t), \quad (23)$$

where

$$H_J(t) = \frac{J(t)}{2}(\sigma_{i,j}^x \sigma_{i,j+1}^x + \sigma_{i,j}^y \sigma_{i,j+1}^y) \quad (24)$$

is the XY interaction Hamiltonian between qubits $Q_{i,j}$ and $Q_{i,j+1}$, with $J(t) = J_0 \sin^2(\pi t/T_3)$ being the time-dependent interaction strength. The Hamiltonian

$$H_{zz3} = \eta_{zz}[\sigma_{i,j}^z Z_{i,j} + \sigma_{i,j+1}^z (Z_{i,j+1} - \sigma_{i,j}^z)] \quad (25)$$

represents the ZZ crosstalk between qubits. The additional Hamiltonian $H_{A3}(t) = i\dot{\mathcal{A}}_3(t)\mathcal{A}_3^\dagger(t)$ is introduced to suppress the ZZ crosstalk.

To achieve the SWAP gate while suppressing ZZ crosstalk by only single-qubit gate correction, we divide the evolution into two steps. In the first step, we choose $\mathcal{A}_{31}(t) = \exp[-i\omega_3\tau_3/\pi \sin^2(\pi t/\tau_3)(\sigma_{i-1,j+1}^x + \sigma_{i,j}^x + \sigma_{i,j+2}^x + \sigma_{i+1,j+1}^x)]$, with $\tau_3 = T_3/4$ (meaning $k = 4$), and $\omega_3 = 4 \times 2.4J_0$. Similar to the single-qubit case, the choice of $\mathcal{A}_{31}(t)$ is still not fixed, it needs to only satisfy the boundary conditions and Eq. (11). Here, for the sake of simplicity, we set \mathcal{A}_{31} in a single-qubit rotation form, making the additional correction term, which is $H_{A3}(t)$ in Eq. (23), just contain single-qubit operations. By rotating the system to the framework defined by $\mathcal{A}_{31}(t)$, we obtain

$$\begin{aligned} H_{A3}^1(t) &= \mathcal{A}_{31}^\dagger(t)H_3(t)\mathcal{A}_{31}(t) + i\dot{\mathcal{A}}_{31}^\dagger(t)\mathcal{A}_{31}(t) \\ &= \frac{J(t)}{2}\sigma_{i,j}^x\sigma_{i,j+1}^x \\ &+ \mathcal{A}_{31}^\dagger(t)\left[\frac{J(t)}{2}\sigma_{i,j}^y\sigma_{i,j+1}^y + H_{zz3}\right]\mathcal{A}_{31}(t), \end{aligned} \quad (26)$$

where $\int_{(n-1)\tau_3}^{n\tau_3} \mathcal{A}_{31}^\dagger(t)[J(t)\sigma_{i,j}^y\sigma_{i,j+1}^y/2 + H_{zz3}]\mathcal{A}_{31}(t)dt = 0$. Hence, when $\int_0^{T_3} J(t)dt = \pi/2$, in the framework of $\mathcal{A}_{31}(t)$, the evolution operator in the first step is $U_{\mathcal{A}_3}^1(T_3, 0) = \exp[-i\pi\sigma_{i,j}^x\sigma_{i,j+1}^x/4]$, which represents a nontrivial two-qubit gate, i.e., we can perform two-qubit gate with suppression of ZZ crosstalk in only one step. By combining arbitrary

single-qubit gate operations, we can achieve universal quantum computation. However, to enable direct comparison with the dynamical gate scheme, we target to construct a SWAP gate. This is because under XY interactions, the dynamical gate scheme can directly implement a SWAP gate instead of $U_{A_3}^1(T_3, 0)$. To build the SWAP gate, we need to proceed with the next step.

In the second step, we choose $\mathcal{A}_{32}(t) = \exp[-i\omega_3\tau_3/\pi \sin^2(\pi t/\tau_3)(\sigma_{i-1,j+1}^y + \sigma_{i,j}^y + \sigma_{i,j+2}^y + \sigma_{i+1,j+1}^y)]$, and the Hamiltonian $H_{A_3}(t)$ in Eq. (23), in the framework defined by $\mathcal{A}_{32}(t)$, is

$$\begin{aligned} H_{A_3}^2(t) &= \mathcal{A}_{32}^\dagger(t)H_3(t)\mathcal{A}_{32}(t) + i\dot{\mathcal{A}}_{32}^\dagger(t)\mathcal{A}_{32}(t) \\ &= \frac{J(t)}{2}\sigma_{i,j}^y\sigma_{i,j+1}^y \\ &+ \mathcal{A}_{32}^\dagger(t)\left[\frac{J(t)}{2}\sigma_{i,j}^x\sigma_{i,j+1}^x + H_{zz3}\right]\mathcal{A}_{32}(t). \end{aligned} \quad (27)$$

Since $\int_{(n-1)\tau_3}^{n\tau_3} \mathcal{A}_{32}^\dagger(t) [J(t)\sigma_{i,j}^x\sigma_{i,j+1}^x/2 + H_{zz3}] \mathcal{A}_{32}(t) dt = 0$, the evolution operator in the second step becomes $U_{A_3}^2(2T_3, T_3) = \exp[-i\pi\sigma_{i,j}^y\sigma_{i,j+1}^y/4]$. As a result, the evolution operator of the whole process is

$$U_{A_3}(2T_3, 0) = U_{A_3}(2T_3, T_3)U_{A_3}(T_3, 0) = U_{(i,j),(i,j+1)}^S, \quad (28)$$

which is a SWAP gate between qubits $Q_{i,j}$ and $Q_{i,j+1}$. Moving back to the interaction picture, the evolution operator generated by $H_3(t)$ at the end time reads

$$U_3(2T_3) = \mathcal{A}_{32}(2T_3)U_{(i,j),(i,j+1)}^S = U_{(i,j),(i,j+1)}^S. \quad (29)$$

Therefore, we realize the two-qubit SWAP gate with ZZCM.

It should be noted that, to suppress ZZ crosstalk, an additional Hamiltonian $H_{A_3}(t) = i\dot{\mathcal{A}}_3(t)\mathcal{A}_3^\dagger(t)$ is introduced, as shown in Eq. (23). This extra Hamiltonian requires additional drives not only on qubit $Q_{i,j}$ but also on spectator qubits $Q_{i-1,j+1}$, $Q_{i,j+2}$, and $Q_{i+1,j+1}$. We emphasize that these spectator qubits do not represent any additional physical qubits overhead on the quantum processor, as we can still perform independent quantum gate operations on them. This means that while implementing the SWAP gate, parallel single-qubit gates on the three qubit can also be obtained simultaneously. To demonstrate this, we introduce a parallel gate $U_{(i,j),(i,j+1)}^S \otimes \sigma_{i-1,j+1}^x \otimes \sigma_{i,j+2}^y \otimes I_{i+1,j+1}$, which consists of a SWAP gate on qubits $Q_{i,j}$ and $Q_{i,j+1}$, a σ^x gate on qubit $Q_{i-1,j+1}$, a σ^y gate on qubit $Q_{i,j+2}$, and an identity gate on qubit $Q_{i+1,j+1}$. In this scenario, the total Hamiltonian is represented as $H_3'(t) = H_3(t) + H_s(t)$, where

$$H_s(t) = \frac{J(t)}{2}(\sigma_{i-1,j+1}^x + \sigma_{i,j+2}^y) \quad (30)$$

is the Hamiltonian for constructing the single-qubit gates.

Figure 3(b) displays the numerically simulated gate fidelity as a function of ZZ crosstalk. The comparison between the performance of ZZCM and DY schemes is presented, where

the latter is implemented via the Hamiltonian of

$$\begin{aligned} H_{d3}(t) &= \frac{J(t)}{2}(\sigma_{i,j}^x\sigma_{i,j+1}^x + \sigma_{i,j}^y\sigma_{i,j+1}^y) \\ &+ J(t)(\sigma_{i-1,j+1}^x + \sigma_{i,j+2}^y), \end{aligned} \quad (31)$$

see Appendix B for details. Figure 3(b) demonstrates that the ZZCM scheme exhibits remarkable robustness against ZZ crosstalk, outperforming the DY scheme. The results reveal that the two-qubit gate is much more sensitive to ZZ crosstalk than the single-qubit gate and that the incorporation of the ZZCM method can efficiently mitigate this issue. Specifically, the incorporation of the ZZCM approach reduces the infidelity of the parallel gate $U_{(i,j),(i,j+1)}^S \otimes \sigma_{i-1,j+1}^x \otimes \sigma_{i,j+2}^y \otimes I_{i+1,j+1}$ by 3 orders of magnitude, compared to the DY scheme, when the ZZ crosstalk ratio is 0.05. Parallel SWAP gates can also be implemented, see Appendix E for details.

IV. DISCUSSION AND CONCLUSION

We have presented a protocol for implementing ZZ -crosstalk-mitigation universal quantum gates in a two-dimensional square lattice. This approach is also applicable to other kinds of lattices, encompassing three-dimensional qubit arrays. It eliminates the need for auxiliary qubits, simplifying the implementation process and reducing resource requirements. Moreover, the method is compatible with different types of quantum processors, accommodating both direct and bus-based qubit interactions. These features contribute to the versatility and scalability of the ZZ -crosstalk mitigation scheme, making it a promising approach for a wide range of quantum computation platforms. By employing a time-dependent unitary transformation operator, we successfully realize high-performance isolated and parallel quantum gates while mitigating the ZZ crosstalk between qubits. Notably, the ZZCM proposal can be utilized to prevent the accumulation and propagation of errors induced by ZZ crosstalk, making it a promising solution for constructing deep quantum circuits and simulating quantum algorithms. Consequently, our protocol may lay the groundwork for practical, scalable, and fault-tolerant quantum computation.

ACKNOWLEDGEMENTS

This work was supported by the National Natural Science Foundation of China (Grant No. 12275090 and No. 12304554), the Guangdong Provincial Key Laboratory (Grant No. 2020B1212060066), the Innovation Program for Quantum Science and Technology (Grant No. 2021ZD0302303), NSFC/RGC JRS (Grant No. N-HKU774/21), and the CRF of Hong Kong (Grant No. C6009-20G).

Appendix A: Numerical Simulation for the Error cumulant

To mitigate the influence of ZZ crosstalk, the time-dependent transformed operator $\mathcal{A}(t)$ needs to satisfy the

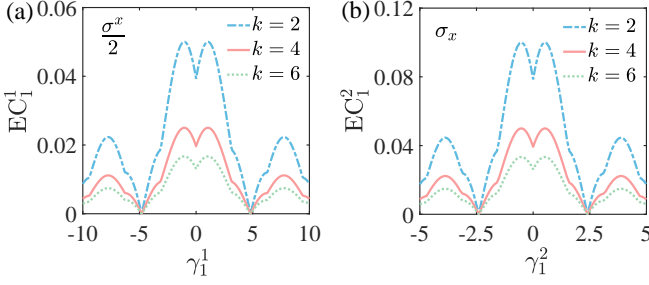


FIG. 4. The error cumulant as a function of γ_1^l , where the optimal values of γ_1^l for isolated $\sigma^x/2$ and σ^x gates are $\gamma_1^l = |4.81|$ and $\gamma_1^l = |2.4|$, respectively, when setting $\eta_{zz} = 0.05\Omega_{01}$.

requirement stated in Eq. (11) of the main text. For single-qubit gates $U_{(l=1,2)}$ ($U_1 = \sigma^x/2$, $U_2 = \sigma^x$) on qubit $Q_{i,j}$, the corresponding operation duration satisfy $\int_0^{T_1^l} \Omega_{01} \sin^2(\pi t/T_1^l) dt = \pi/4$ and $\int_0^{T_2^l} \Omega_{01} \sin^2(\pi t/T_2^l) dt = \pi/2$, respectively. The Hamiltonian describing the ZZ crosstalk between nearest qubits reads in Eq. (14). To mitigate the ZZ crosstalk from nearest qubits, we choose $\mathcal{A}_1^l(t) = \exp[-i\omega_1^l \tau_1^l / \pi \sin^2(\pi t/\tau_1^l) \sigma_{i,j}^x]$, where $\tau_1^l = T_1^l/k$ is the period, and $\omega_1^l = \gamma_1^l k \Omega_{01}$ (k is positive integer) is the parameter used to satisfy Eq. (11b). Therefore, the condition in Eq. (11b) can be expressed as

$$\begin{aligned} & \int_{(n-1)\tau_1^l}^{n\tau_1^l} \mathcal{A}_1^l(t) H_{zz1} \mathcal{A}_1^l(t) dt \\ &= \eta_{zz} \int_{(n-1)\tau_1^l}^{n\tau_1^l} (\cos \chi_1^l \sigma_{i,j}^z + \sin \chi_1^l \sigma_{i,j}^y) Z_{i,j} dt, \end{aligned} \quad (\text{A1})$$

where $\chi_1^l = 2\gamma_1^l k \Omega_{01} \tau_1^l / \pi \sin^2(\pi t/\tau_1^l)$. We define the error cumulant during the n th period as

$$\text{EC}_1^l = \eta_{zz} \left[\left| \int_{(n-1)\tau_1^l}^{n\tau_1^l} \cos \chi_1^l dt \right| + \left| \int_{(n-1)\tau_1^l}^{n\tau_1^l} \sin \chi_1^l dt \right| \right]. \quad (\text{A2})$$

Figures 4(a) and (b) display the error cumulant as a function of γ_1^l , indicating that for the $\sigma^x/2$ (σ^x) gate, $\gamma_1^l = |4.81|$ ($\gamma_1^l = |2.4|$) is the optimal choice for eliminating the ZZ crosstalk.

After setting γ_1 , the shape of the modulated amplitude $\Omega_1(t)$ for different values of k can be determined, as shown in Fig. 5. The modulated $\Omega_1(t)$ is presented in Eq. (18), with $\Omega_1(t) = \Omega_{01} \sin^2(\pi t/T_1) + \omega_1 \sin(2\pi t/\tau_1)$, and $\omega_1 = \gamma_1 k \Omega_{01}$. As ω_1 is proportional to k , the effective maximum amplitude of $\Omega_1(t)$ will be larger than the original driving field. Despite this limitation, as numerically verified, the gate performance can still be greatly improved. In addition, the modulated drive maintains the waveform of the original field as a simple periodic function and can be readily obtained experimentally by arbitrary waveform generators [41, 42].

For the parallel single-qubit gate on next-nearest-neighbor qubits $Q_{i,j}$ and $Q_{i+1,j+1}$, the ZZ -crosstalk Hamiltonian is in the form in Eq. (20). The gate operation time T_2 satisfies

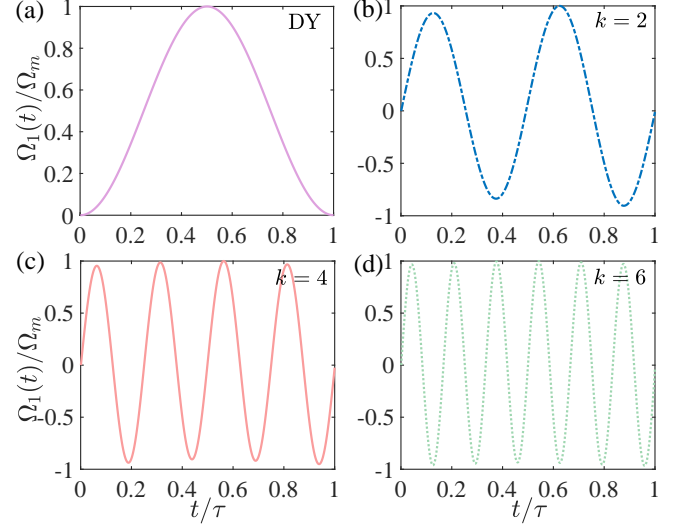


FIG. 5. The waveform of the modulated drive $\Omega_1(t)$ for the $\sigma^x/2$ gate, (a) in the dynamical gate scheme and (b)-(d) in our ZZCM scheme with $\gamma_1^l = 4.81$ and different k .

$\int_0^{T_2} \Omega_{02} \sin^2(\pi t/T_2) dt = \pi/2$. When we choose the transformed operator in the form in Eq. (21), with $\tau_2 = T_2/k$ being the period, and $\omega_2 = \gamma_2 k \Omega_{02}$ used to satisfy Eq. (11b). In this case, the condition in Eq. (11b) can be written as

$$\begin{aligned} & \int_{(n-1)\tau_2}^{n\tau_2} \mathcal{A}_2^\dagger(t) H_{zz2} \mathcal{A}_2(t) dt \\ &= \eta_{zz} \left[\int_{(n-1)\tau_2}^{n\tau_2} (\cos \chi_2 \sigma_{i,j}^z + \sin \chi_2 \sigma_{i,j}^y) Z_{i,j} dt \right. \\ & \quad \left. + \int_{(n-1)\tau_2}^{n\tau_2} (\cos \chi_2 \sigma_{i+1,j+1}^z - \sin \chi_2 \sigma_{i+1,j+1}^x) Z_{i+1,j+1} dt \right], \end{aligned} \quad (\text{A3})$$

with $\chi_2 = 2\gamma_2 k \Omega_{02} \tau_2 / \pi \sin^2(\pi t/\tau_2)$. We can also define the error cumulant during the n th period as

$$\text{EC}_2 = \eta_{zz} \left[\left| \int_{(n-1)\tau_2}^{n\tau_2} \cos \chi_2 dt \right| + \left| \int_{(n-1)\tau_2}^{n\tau_2} \sin \chi_2 dt \right| \right], \quad (\text{A4})$$

which is consistent with the error cumulant in isolated σ^x gate.

Appendix B: The construction of dynamical gates

Here, we present the construction of dynamical (DY) gates with simple resonant interaction. They are implemented by using time-dependent driving fields, and the corresponding Hamiltonians are $H_{d1}(t) = \Omega_d \sin^2(\pi t/T_{d1}) \sigma_{i,j}^x$ and $H_{d2}(t) = \Omega_d \sin^2(\pi t/T_{d2}) (\sigma_{i,j}^x + \sigma_{i',j'}^y)$ for single-qubit gate on qubit $Q_{i,j}$, and parallel single-qubit gate $\sigma_{i,j}^x \otimes \sigma_{i',j'}^y$ between nearest or next-nearest neighboring qubits $Q_{i,j}$ and $Q_{i',j'}$, respectively. To construct the isolated gate $\sigma^x/2$ (σ^x), the corresponding evolution time T_{d1}

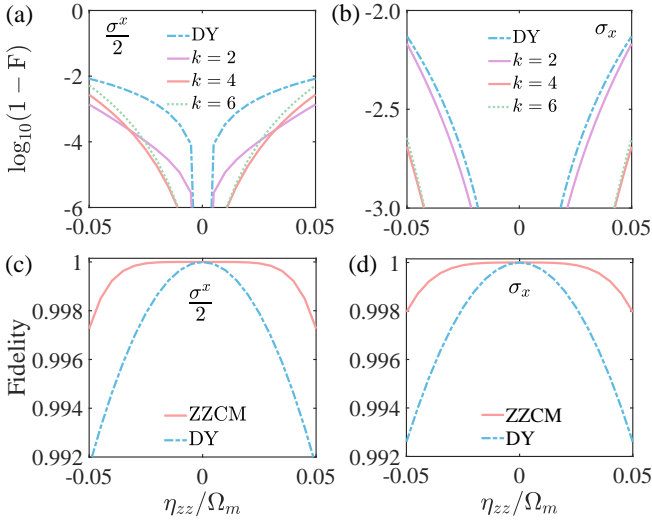


FIG. 6. (a) and (b) display the infidelity of isolated $\sigma^x/2$ and σ^x gates for various k under the condition that the maximum equivalent coupling strength is Ω_m , as a function of η_{zz}/Ω_m . (c) and (d) compare the robustness of isolated $\sigma^x/2$ and σ^x gates of the ZZCM scheme with $k = 4$ and the DY scheme.

satisfies $\int_0^{T_{d1}} \Omega_d \sin^2(\pi t/T_{d1}) dt = \pi/4$ ($\pi/2$). Similarly, for the parallel single-qubit gate, the evolution time is $\int_0^{T_{d2}} \Omega_d \sin^2(\pi t/T_{d2}) dt = \pi/2$. The amplitude of the driven field is set to be equal to the amplitude of the equivalent coupling strength in the ZZCM scheme, i.e., $\Omega_d = \Omega_m$.

We also present the implementation of the two-qubit SWAP gate using a simple XY interaction. The corresponding Hamiltonian is given by

$$H_{d3}(t) = J_d(t)(\sigma_{i,j}^x \sigma_{i',j'}^x + \sigma_{i,j}^y \sigma_{i',j'}^y)/2, \quad (\text{B1})$$

where $J_d(t) = J_0 \sin^2(\pi t/T_{d3})$ is the time-dependent XY interaction between qubits $Q_{i,j}$ and $Q_{i',j'}$, and the evolution time satisfies $\int_0^{T_{d3}} J_d(t) dt = \pi/2$.

Moreover, we construct parallel gates of $U_{(i,j),(i,j+1)}^S \otimes \sigma_{i-1,j+1}^x \otimes \sigma_{i,j+2}^y \otimes I_{i+1,j+1}$ and $U_{(i,j),(i,j+1)}^S \otimes U_{(i+1,j),(i+1,j+1)}^S$ by using the DY method. The corresponding Hamiltonian is given by Eq. (31) and

$$H_{d5}(t) = \frac{J_d(t)}{2} (\sigma_{i,j}^x \sigma_{i,j+1}^x + \sigma_{i,j}^y \sigma_{i,j+1}^y + \sigma_{i+1,j}^x \sigma_{i+1,j+1}^x + \sigma_{i+1,j}^y \sigma_{i+1,j+1}^y), \quad (\text{B2})$$

respectively, where the evolution time is chosen to satisfy $\int_0^{T_{d4(5)}} J_d(t) dt = \pi/2$. We note that the form of the ZZ -crosstalk Hamiltonian is the same as in the ZZCM scheme.

Appendix C: The Optimal k for the ZZCM Scheme

We draw attention to the incorporation of the ZZCM control, which induces an increase in the effective coupling strength as k grows, as established by Eq. (18) in the main

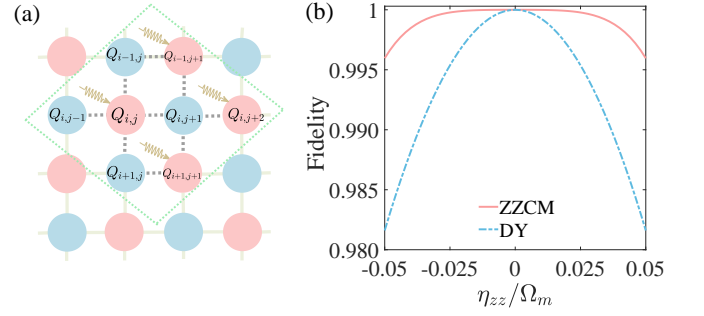


FIG. 7. Implementation of parallel single-qubit gates. (a) Schematic diagram for $\sigma_{i,j}^x \otimes \sigma_{i,j+1}^y$ gates between nearest qubits $Q_{i,j}$ and $Q_{i,j+1}$. (b) compares the robustness of the parallel gate $\sigma_{i,j}^x \otimes \sigma_{i,j+1}^y$ between the ZZCM scheme with $k = 4$ and the DY scheme.

paper. The corresponding equivalent coupling strength for the ZZCM approach is provided by $\Omega_1(t) = \Omega_{01} \sin^2(\pi t/T_1) + \omega_1 \sin(2\pi t/\tau_1)$, where $\omega_1 = \gamma_1 k \Omega_{01}$. To prevent excessive driving field amplitude in experiments, the amplitude of the equivalent coupling strength is constrained to Ω_m , and the ZZ crosstalk ratio η_{zz}/Ω_m is within the range of $[-0.05, 0.05]$. Under these conditions, as k increases, the gate-driven field amplitude Ω_{01} diminishes, consequently resulting in increased relative noise, quantified by the parameter η_{zz}/Ω_{01} . Therefore, there exists a trade-off between the enhancement in robustness with increasing k and the proportion of noise η_{zz}/Ω_{01} . Figures 6(a) and (b) depict the infidelities of $\sigma^x/2$ and σ^x gates, respectively, as a function of η_{zz}/Ω_m , with an optimal value of $k = 4$ identified for the ZZCM scheme. Additionally, Figs. 6(c) and (d) contrast the robustness of the ZZCM scheme, with $k = 4$, against the DY scheme concerning ZZ crosstalk when the equivalent coupling strength amplitude is Ω_m . The plots distinctly showcase the outstanding suppression of ZZ crosstalk achieved by the ZZCM scheme.

Appendix D: The construction of parallel gates on nearby qubits

Here, we present the construction of parallel single-qubit gate between nearest-neighbor qubits in an eight-qubit system, which is enclosed by the dotted box in Fig. 7(a). We apply σ^x and σ^y gates simultaneously on qubits $Q_{i,j}$ and $Q_{i,j+1}$, and the remaining six qubits serve as spectators. Starting from Eq. (10) in the main text, the individual single-qubit-driven Hamiltonian in the \mathcal{A} framework is $H'_{\mathcal{A}2}(t) = \Omega_{02} \sin^2(\pi t/T_2)(\sigma_{i,j}^x + \sigma_{i,j+1}^y)$, and the ZZ interaction Hamiltonian is

$$H'_{zz2} = \eta_{zz} [\sigma_{i,j}^z Z_{i,j} + \sigma_{i,j+1}^z (Z_{i,j+1} - \sigma_{i,j}^z)]. \quad (\text{D1})$$

To suppress the ZZ crosstalk between qubits, we choose

$$\mathcal{A}'_2(t) = \exp \left[-i \frac{\omega_2 \tau_2}{\pi} \sin^2 \left(\frac{\pi t}{\tau_2} \right) (\sigma_{i-1,j+1}^x + \sigma_{i,j}^x + \sigma_{i,j+2}^x + \sigma_{i+1,j+1}^x) \right]. \quad (\text{D2})$$

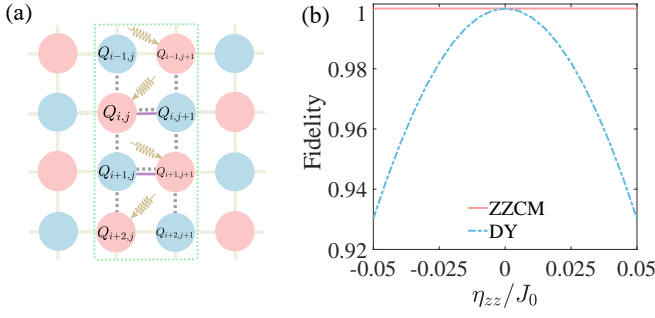


FIG. 8. Implementation of two-qubit gates. (a) shows the schematic diagrams for the parallel gated $U_{(i,j),(i,j+1)}^S \otimes U_{(i+1,j),(i+1,j+1)}^S$. (b) compares the robustness between the ZZCM scheme with $k = 4$ and the DY scheme, respectively.

The total Hamiltonian,

$$H'_2(t) = H_{zz2} + \Omega_2(t)\sigma_{i,j}^x + \Omega_{02} \sin^2\left(\frac{\pi t}{T_2}\right) \sigma_{i,j+1}^y + \Omega_A(\sigma_{i-1,j+1}^x + \sigma_{i,j+2}^x + \sigma_{i+1,j+1}^x), \quad (\text{D3})$$

in the interaction picture can be obtained by inverting Eq. (4) of the main text, where $\Omega_A = \omega_2 \sin(2\pi t/\tau_2)$, and $\Omega_2(t) = \Omega_{02} \sin^2(\pi t/T_2) + \Omega_A$ is the equivalent coupling strength applying on qubit $Q_{i,j}$. It indicates that, for mitigating ZZ crosstalk, we need additional control fields apply on qubits $Q_{i-1,j+1}$, $Q_{i,j}$, $Q_{i,j+2}$, and $Q_{i+1,j+1}$. However, it is worth noting that qubits $Q_{i-1,j+1}$, $Q_{i,j+2}$, and $Q_{i+1,j+1}$ do not incur extra resource consumption on the quantum processor as we can still implement single-qubit gates independently on these qubits.

We conduct a comparative analysis of the ZZCM scheme and the DY scheme, focusing on their robustness against ZZ crosstalk. We here impose a constraint on the maximum value of the equivalent coupling strength $\Omega_2(t)$, limiting it to Ω_m . Comparing Fig. 7(b) and Figs. 6(c) and (d), we observe that the susceptibility of the parallel single-qubit gate to ZZ crosstalk exceeds that of isolated single-qubit gates. Fortunately, the proposed ZZCM scheme effectively mitigates the adverse effects of ZZ crosstalk. Consequently, the parallel single-qubit gate achieves comparable performance to isolated

single-qubit gates.

Appendix E: The construction of parallel SWAP gates

We next demonstrate the application of the ZZCM control for realizing the parallel two-qubit SWAP gate in an eight-qubit system, as shown in the dotted box in Fig. 8(a). The SWAP gates on qubits $Q_{i,j}$ and $Q_{i,j+1}$, $Q_{i+1,j}$ and $Q_{i+1,j+1}$ are implemented by turning on the XY interaction between the respective qubit pairs. The total Hamiltonian of this quantum system in the interaction picture is

$$H_4(t) = H'_J(t) + H_{zz4} + H'_A(t), \quad (\text{E1})$$

which is composed of the XY interaction Hamiltonian

$$H'_J(t) = \frac{J(t)'}{2} (\sigma_{i,j}^x \sigma_{i,j+1}^x + \sigma_{i,j}^y \sigma_{i,j+1}^y + \sigma_{i+1,j}^x \sigma_{i+1,j+1}^x + \sigma_{i+1,j}^y \sigma_{i+1,j+1}^y) \quad (\text{E2})$$

between qubits $Q_{i,j}$ and $Q_{i,j+1}$, $Q_{i+1,j}$ and $Q_{i+1,j+1}$, with $J(t)' = J_0 \sin^2(\pi t/T_4)$ as the time-dependent interaction strength. The ZZ-crosstalk Hamiltonian in this system is described by $H_{zz4} = \eta_{zz} [\sigma_{i,j}^z (Z_{i,j} - \sigma_{i,j-1}^z) + \sigma_{i,j+1}^z (\sigma_{i-1,j+1}^z + \sigma_{i+1,j+1}^z) + \sigma_{i+1,j}^z (\sigma_{i+1,j+1}^z + \sigma_{i+2,j}^z) + \sigma_{i+1,j+1}^z \sigma_{i+2,j+1}^z]$. To suppress the ZZ crosstalk, we use the additional Hamiltonian $H'_A(t) = i\hat{A}_4(t)\hat{A}_4^\dagger(t)$.

The procedure of constructing the parallel SWAP gate shares similarities with the construction process of an isolated SWAP gate. However, there is a key difference lies in the selection of transformed operator $\mathcal{A}(t)$. Specifically, we select $\mathcal{A}_{41}(t) = \exp[-i\omega_4\tau_4/\pi \sin^2(\pi t/\tau_4)(\sigma_{i-1,j+1}^x + \sigma_{i,j}^x + \sigma_{i+1,j+1}^x + \sigma_{i+2,j}^x)]$ in the first step, followed by $\mathcal{A}_{42}(t) = \exp[-i\omega_4\tau_4/\pi \sin^2(\pi t/\tau_4)(\sigma_{i-1,j+1}^y + \sigma_{i,j}^y + \sigma_{i+1,j+1}^y + \sigma_{i+2,j}^y)]$ in the second step, with $\tau_4 = T_4/k$, and $\omega_4 = 2.4kJ_0$. Under these settings, the ZZCM scheme exhibits superior robustness against ZZ crosstalk as expected, as shown in Fig. 8(b). In contrast, the gate fidelity experiences a rapid decline as η_{zz}/J_0 increases when the ZZCM control is absent. However, by employing the ZZCM method, we successfully enhance the fidelity of the parallel SWAP gate from an initial value of 93.02% to 99.99% when the ZZ-crosstalk ratio is $\eta_{zz}/J_0 = |0.05|$.

- [1] L. M. K. Vandersypen, M. Steffen, G. Breyta, C. S. Yannoni, M. H. Sherwood, and I. L. Chuang, Experimental realization of Shor's quantum factoring algorithm using nuclear magnetic resonance, *Nature (London)* **414**, 883 (2001).
- [2] E. Lucero, R. Barends, Y. Chen, J. Kelly, M. Mariantoni, A. Megrant, P. O'Malley, D. Sank, A. Vainsencher, J. Wenner, T. White, Y. Yin, A. N. Cleland, and J. M. Martinis, Computing prime factors with a Josephson phase qubit quantum processor, *Nat. Phys.* **8**, 719 (2012).
- [3] J. A. Jones, M. Mosca, and R. H. Hansen, Implementation of a quantum search algorithm on a quantum computer, *Nature (London)* **393**, 344 (1998).

- [4] A. Rodriguez-Blanco, A. Bermudez, M. Müller, and F. Shahandeh, Efficient and robust certification of genuine multipartite entanglement in noisy quantum error correction circuits, *PRX Quantum* **2**, 020304 (2021).
- [5] P. Zhao, K. Linghu, Z. Li, P. Xu, R. Wang, G. Xue, Y. Jin, and H. Yu, Quantum Crosstalk Analysis for Simultaneous Gate Operations on Superconducting Qubits, *PRX Quantum* **3**, 020301 (2022).
- [6] D. Buterakos, R. E. Throckmorton, and S. D. Sarma, Crosstalk error correction through dynamical decoupling of single-qubit

- gates in capacitively coupled singlet-triplet semiconductor spin qubits, *Phys. Rev. B* **97**, 045431 (2018).
- [7] R. E. Throckmorton and S. Das Sarma, Crosstalk- and charge-noise-induced multiqubit decoherence in exchange-coupled quantum dot spin qubit arrays, *Phys. Rev. B* **105**, 245413 (2022).
- [8] A. Kandala, K. X. Wei, S. Srinivasan, E. Magesan, S. Carnevale, G. A. Keefe, D. Klaus, O. Dial, and D. C. McKay, Demonstration of a High-Fidelity CNOT Gate for Fixed-Frequency Transmons with Engineered ZZ Suppression, *Phys. Rev. Lett.* **127**, 130501 (2021).
- [9] L. Postler, Á. Rivas, P. Schindler, A. Erhard, R. Stricker, D. Nigg, T. Monz, R. Blatt, and M. Müller, Experimental quantification of spatial correlations in quantum dynamics, *Quantum* **2**, 90 (2018).
- [10] U. von Lüpke, F. Beaudoin, L. M. Norris, Y. Sung, R. Winik, J. Y. Qiu, M. Kjaergaard, D. Kim, J. Yoder, S. Gustavsson, L. Viola, and W. D. Oliver, Two-qubit spectroscopy of spatiotemporally correlated quantum noise in superconducting qubits, *PRX Quantum* **1**, 010305 (2020).
- [11] N. Sundaresan, I. Lauer, E. Pritchett, E. Magesan, P. Jurcevic, and J. M. Gambetta, Reducing unitary and spectator errors in cross resonance with optimized rotary echoes, *PRX Quantum* **1**, 020318 (2020).
- [12] S. Krinner, S. Lazar, A. Remm, C. K. Andersen, N. Lacroix, G. J. Norris, C. Hellings, M. Gabureac, C. Eichler, and A. Wallraff, Benchmarking Coherent Errors in Controlled-Phase Gates due to Spectator Qubits, *Phys. Rev. Appl.* **14**, 024042 (2020).
- [13] T. Q. Cai, X. Y. Han, Y. K. Wu, Y. L. Ma, J. H. Wang, Z. L. Wang, H. Y. Zhang, H. Y. Wang, Y. P. Song, and L. M. Duan, Impact of Spectators on a Two-Qubit Gate in a Tunable Coupling Superconducting Circuit, *Phys. Rev. Lett.* **127**, 060505 (2021).
- [14] P. Mundada, G. Zhang, T. Hazard, and A. Houck, Suppression of Qubit Crosstalk in a Tunable Coupling Superconducting Circuit, *Phys. Rev. Appl.* **12**, 054023 (2019).
- [15] X. Y. Han, T. Q. Cai, X. G. Li, Y. K. Wu, Y. W. Ma, Y. L. Ma, J. H. Wang, H. Y. Zhang, Y. P. Song, and L. M. Duan, Error analysis in suppression of unwanted qubit interactions for a parametric gate in a tunable superconducting circuit, *Phys. Rev. A* **102**, 022619 (2020).
- [16] X. Li, T. Cai, H. Yan, Z. Wang, X. Pan, Y. Ma, W. Cai, J. Han, Z. Hua, X. Han, Y. Wu, H. Zhang, H. Wang, Y. Song, L. Duan, and L. Sun, Tunable Coupler for Realizing a Controlled-Phase Gate with Dynamically Decoupled Regime in a Superconducting Circuit, *Phys. Rev. Appl.* **14**, 024070 (2020).
- [17] M. C. Collodo, J. Herrmann, N. Lacroix, C. K. Andersen, A. Remm, S. Lazar, J.-C. Besse, T. Walter, A. Wallraff, and C. Eichler, Implementation of Conditional Phase Gates Based on Tunable ZZ Interactions, *Phys. Rev. Lett.* **125**, 240502 (2020).
- [18] J. Chu and F. Yan, Coupler-Assisted Controlled-Phase Gate with Enhanced Adiabaticity, *Phys. Rev. Appl.* **16**, 054020 (2021).
- [19] P. Zhao, D. Lan, P. Xu, G. Xue, M. Blank, X. Tan, H. Yu, and Y. Yu, Suppression of Static ZZ Interaction in an All-Transmon Quantum Processor, *Phys. Rev. Appl.* **16**, 024037 (2021).
- [20] J. Stehlik, D. M. Zajac, D. L. Underwood, T. Phung, J. Blair, S. Carnevale, D. Klaus, G. A. Keefe, A. Carniol, M. Kumph, M. Steffen, and O. E. Dial, Tunable Coupling Architecture for Fixed-Frequency Transmon Superconducting Qubits, *Phys. Rev. Lett.* **127**, 080505 (2021).
- [21] Y. Sung, L. Ding, J. Braumüller, A. Vepsäläinen, B. Kannan, M. Kjaergaard, A. Greene, G. O. Samach, C. McNally, D. Kim, A. Melville, B. M. Niedzielski, M. E. Schwartz, J. L. Yoder, T. P. Orlando, S. Gustavsson, and W. D. Oliver, Realization of High-Fidelity CZ and ZZ-Free iSWAP Gates with a Tunable Coupler, *Phys. Rev. X* **11**, 021058 (2021).
- [22] J. Ku, X. Xu, M. Brink, D. C. McKay, J. B. Hertzberg, M. H. Ansari, and B. L. T. Plourde, Suppression of Unwanted ZZ Interactions in a Hybrid Two-Qubit System, *Phys. Rev. Lett.* **125**, 200504 (2020).
- [23] P. Zhao, P. Xu, D. Lan, J. Chu, X. Tan, H. Yu, and Y. Yu, High-Contrast ZZ Interaction Using Superconducting Qubits with Opposite-Sign Anharmonicity, *Phys. Rev. Lett.* **125**, 200503 (2020).
- [24] X. Xu and M. H. Ansari, ZZ Freedom in Two-Qubit Gates, *Phys. Rev. Appl.* **15**, 064074 (2021).
- [25] A. Noguchi, A. Osada, S. Masuda, S. Kono, K. Heya, S. P. Wolski, H. Takahashi, T. Sugiyama, D. Lachance-Quirion, and Y. Nakamura, Fast parametric two-qubit gates with suppressed residual interaction using the second-order non-linearity of a cubic transmon, *Phys. Rev. A* **102**, 062408 (2020).
- [26] B. K. Mitchell, R. K. Naik, A. Morvan, A. Hashim, J. M. Kreikebaum, B. Marinelli, W. Lavrijsen, K. Nowrouzi, D. I. Santiago, and I. Siddiqi, Hardware-Efficient Microwave-Activated Tunable Coupling between Superconducting Qubits, *Phys. Rev. Lett.* **127**, 200502 (2021).
- [27] H. Xiong, Q. Ficheux, A. Somoroff, L. B. Nguyen, E. Dogan, D. Rosenstock, C. Wang, K. N. Nesterov, M. G. Vavilov, and V. E. Manucharyan, Arbitrary controlled-phase gate on fluxonium qubits using differential ac stark shifts, *Phys. Rev. Res.* **4**, 023040 (2022).
- [28] K. X. Wei, E. Magesan, I. Lauer, S. Srinivasan, D. F. Bogorin, S. Carnevale, G. A. Keefe, Y. Kim, D. Klaus, W. Landers, N. Sundaresan, C. Wang, E. J. Zhang, M. Steffen, O. E. Dial, D. C. McKay, and A. Kandala, Quantum crosstalk cancellation for fast entangling gates and improved multi-qubit performance, arXiv:2106.00675.
- [29] Z. C. Ni, S. Li, L. B. Zhang, J. Chu, J. J. Niu, T. X. Yan, X. H. Deng, L. Hu, J. Li, Y. P. Zhong, S. Liu, F. Yan, Y. Xu, and D. P. Yu, Scalable Method for Eliminating Residual ZZ Interaction between Superconducting Qubits, *Phys. Rev. Lett.* **129**, 040502 (2022).
- [30] L. Viola, S. Lloyd, and E. Knill, Dynamical Decoupling of Open Quantum Systems, *Phys. Rev. Lett.* **82**, 2417(1999).
- [31] D. Suter and G. A. Álvarez, Protecting quantum information against environmental noise, *Rev. Mod. Phys.* **88**, 041001 (2016).
- [32] P. Jurcevic, A. Javadi-Abhari, L. S. Bishop, I. Lauer, D. F. Bogorin, M. Brink, L. Capelluto, O. Günlük, T. Itoko, and N. Kanazawa, Demonstration of quantum volume 64 on a superconducting quantum computing system, *Quantum Sci. Technol.* **6**, 025020 (2021).
- [33] V. Tripathi, H. Chen, M. Khezri, K.-W. Yip, E. M. Levenson-Falk, and D. A. Lidar, Suppression of crosstalk in superconducting qubits using dynamical decoupling, *Phys. Rev. Appl.* **18**, 024068 (2022).
- [34] Z. Y. Zhou, R. Sitler, Y. Oda, K. Schultz, and G. Quiroz, Quantum Crosstalk Robust Quantum Control, *Phys. Rev. Lett.* **131**, 210802 (2023).
- [35] A. Imamoglu, D. D. Awschalom, G. Burkard, D. P. DiVincenzo, D. Loss, M. Sherwin, and A. Small, Quantum Information Processing Using Quantum Dot Spins and Cavity QED, *Phys. Rev. Lett.* **83**, 4204 (1999).
- [36] P. Jurcevic, B. P. Lanyon, P. Hauke, C. Hempel, P. Zoller, R. Blatt, and C. F. Roos, Quasiparticle Engineering and Entanglement Propagation in a Quantum Many-Body System, *Nature (London)* **511**, 202 (2014).

- [37] W. Magnus, On the Exponential Solution of Differential Equations for a Linear Operator, *Commun. Pure Appl. Math.* **7**, 649 (1954).
- [38] S. Blanes, F. Casas, J. A. Oteo, and J. Ros, The Magnus Expansion and Some of Its Applications, *Phys. Rep.* **470**, 151 (2009).
- [39] A. Bermudez, F. Jelezko, M. B. Plenio, and A. Retzker, Electron-Mediated Nuclear-Spin Interactions between Distant Nitrogen-Vacancy Centers, *Phys. Rev. Lett.* **107**, 150503 (2011).
- [40] X. G. Wang, Z. Sun, and Z. D. Wang, Operator fidelity susceptibility: An indicator of quantum criticality, *Phys. Rev. A* **79**, 012105 (2009).
- [41] S. T. Cundiff, A. M. Weiner, Optical arbitrary waveform generation, *Nat. Photonics* **4**, 760(2010).
- [42] K. Takase, A. Kawasaki, B. K. Jeong, et al, Quantum arbitrary waveform generator, *Sci. Adv.* **8**, eadd4019 (2022).